Publ. Natl. Astron. Obs. Japan Vol. 13. 57 − 69 (2010)

Performance of VERA in the Phase-Referencing Astrometry

Mareki HONMA[1,2], Tomoya HIROTA[1,2], Takaaki JIKE[1,2], Osamu KAMEYA[1,2], Noriyuki KAWAGUCHI[1,2], Hideyuki KOBAYASHI[1,2], Tomoharu KURAYAMA[3], Seiji MANABE[1,2], Takeshi MIYAJI[1], Takumi NAGAYAMA[1], Kotaro NIINUMA[1], Toshihiro OMODAKA[3], Tomoaki OYAMA[1], Katsuhisa SATO[1], Katsunori M. SHIBATA[1,2], Yoshiaki TAMURA[1,2]

(Received 2010 Dec. 6; accepted 2011 Jan. 15)

Abstract

In order to evaluate the performance of VERA in the phase-referencing astrometry, we review the details of the calibrations and data reductions in VERA's astrometry. We present examples of phase-referencing data as well as the results of data reductions, especially focusing on the phase residuals after the phase-referencing. We show that once the calibration processes are carried out in a proper manner, the phase residual after the phase-referencing becomes white-phase noise for nearly full track (i.e., 8 hour), confirming and extending the previous findings for a shorter range (～hour). We also discuss the astrometric accuracy that can be achieved with VERA by considering various sources of errors including both calibration errors in the observing system and the structural effects of objects. In the absence of the structural effect, we show that the tropospheric zenith delay is the dominant source of astrometric error, and also show that parallax measurements at 10 μas level are feasible for sources under good observing conditions (i.e., bright source, close separation, and relatively high declination). On the other hand, based on the most up-to-date results from VERA, we find that the maser structure effect is also significant in many cases, limiting the parallax accuracy at 5-15% level, especially for nearby sources within a few kpc from the Sun.

Key words: astrometry, VLBI, phase-referencing, VERA

1. Introduction

VERA (VLBI Exploration of Radio Astrometry) is a dedicated VLBI array to the phase-referencing astrometry, consisting of four of 20-m diameter telescopes located at Mizusawa, Iriki, Ogasawara and Ishigaki-jima (Sasao 1996; Honma et al. 2000). Based on the dual-beam system with which one can simultaneously observe two adjacent sources in the sky plane, VERA measures the parallaxes and proper motions of Galactic maser sources (H_2O at 22GHz and SiO at 43GHz) by referring to extra-galactic radio sources such as QSOs and radio galaxies. By observing several hundreds to a thousand maser sources, VERA will reveal the three-dimensional structure and dynamics of the Milky Way Galaxy. The construction of the array was completed in 2002 and regular operations of the array started since 2004. To date, observations of ～100 target maser sources have been already conducted, and the astrometric results were published for a few tens of sources (see, for example, papers in PASJ special issues in 2008 & 2011). Since the astrometric results are now obtainable on regular bases with VERA, it is worthy to review the details of phase-referencing analyses in VERA as well as the astrometric accuracy currently achieved. For this purpose, here we summarize the analyses of VERA's phase referencing by showing examples, and evaluate the performance of VERA in phase-referencing astrometry.

[1] Mizusawa VLBI Observatory, NAOJ, Mizusawa, 023-0861
[2] Graduate University for Advanced Studies, Mitaka, 181-8588
[3] Graduate School of Science and Engineering, Kagoshima University, Korimoto, Kagoshima 890-0065 (MH) mareki.honma@nao.ac.jp

2. Calibrations and Data Reductions

In this section we briefly summarize the procedures of calibrations and reductions of the phase-referencing VLBI data obtained with VERA.

2.1. Calibrations

In conducting phase-referencing VLBI astrometry, several calibration processes are required including amplitude calibration, calibrations of delays in troposphere, ionosphere and instruments, and also calibrations of delay model in case that the delay model used for correlation is not precise enough for astrometry, which is the case for VERA.

First, the amplitude calibrations in VERA are performed by measuring the system temperature T^*_{sys}. During the observations, the receiver output power toward the sky is monitored, and the system noise temperature (including the sky and receiver noises) is calibrated with the chopper-wheel on which a dummy load at the room temperature is attached. This method, based on the assumption that the room

temperature of the dummy load is the same to the sky temperature, provides the system noise temperature T^*_{sys} which is corrected for the tropospheric attenuation. In the VERA system, the calibration with the chopper-wheel is done every hour or more, and the receiver output and thus T^*_{sys} are monitored every ten seconds. This method provides the amplitude accuracy of 10-15% level.

In VERA, the use of two independent receivers for the observations of pair sources introduces a path length difference in the instruments (receivers, cables, backends etc.), and this path length difference must be calibrated for conducting accurate astrometry with VERA. For doing the dual-beam delay calibration, we use the horn-on-dish method (Kawaguchi et al. 2000; Honma et al. 2008a), in which a common noise source located near the telescope main reflector is observed with the dual-beam receivers and correlated on real-time to trace the path length difference as well as its variation during the observations. The details of this calibration procedure is summarized in Honma et al. (2008a), showing that the delay difference between the dual-beam receivers can be calibrated at 0.1 mm level.

Since the delay model used in the Mitaka FX correlator, which is the main correlator for VERA, is not accurate enough for VLBI astrometry, we need to recalculate the precise delay. This recalculation is conducted based on the up-to-date geodynamical model described in IERS 1996 (McCarthy 1996), which is thought to have an accuracy better than a few mm. For the delay calculations, the Earth orientation parameter (EOP) is also necessary, and we use the EOP reported in the IERS bulletin B final values[1], which is the current best estimate of EOP utilizing several modern techniques such as VLBI, GPS etc.

The tropospheric delay offset also causes an error in delay calculation and thus to be corrected for accurately. While the short-term fluctuation can be cancelled out with the dual-beam observations (e.g., Honma et al. 2003; see also the next section in this paper), the tropospheric delay offset remains even after the phase-referencing between a pair of adjacent sources, because there is a small air-mass difference between the two sources. Usually this term is described by a combination of the tropospheric zenith delay offset and the mapping function, and using the simplest plane-parallel model for the troposphere, one may write the excess delay as

$$\tau_{trp} = \tau_{trp,0} \sec Z, \quad (1)$$

where $\tau_{trp,0}$ is the tropospheric delay at the zenith, and Z is the zenith angle. To calibrate this delay, the zenith delay $\tau_{trp,0}$ should be measured by some means. In VERA, we have GPS receiving system at each site, and based on the GPS data the tropospheric zenith delay at each station is measured every 5 min. Detailed analyses and comparison with other techniques to measure the tropospheric zenith delay provided that GPS technique can calibrate the zenith delay at ~2 cm level, as discussed in detail in Honma et al. (2008b).

The ionosphere also causes an additional delay in propagation of electro-magnetic wave, and its uncertainty causes error in astrometry. Since the effect of the ionosphere is dispersive and scales with ν^{-2}, at the main bands of VERA (22 GHz and 43 GHz) its effect is not so significant as troposphere. However, it should be also calibrated to conduct high-accuracy astrometry, and for doing this, in VERA we use the Global Ionosphere Map (GIM) such as produced by NASA/GSFC or University of Bern etc.

We note that in practice, the precise measurements of tropospheric and ionospheric delays are included in the delay recalculation, and calibrated together at one time, by correcting for differences of the crude delay in the correlation and precise delay recalculated along with the most up-to-date EOP, GPS-based troposphere and ionosphere.

2.2. Data Reductions

Data reductions in VERA are conducted in a standard manner of phase-referencing VLBI. First the amplitude calibration is done based on the system noise temperature T^*_{sys} measured during the observations. The delay calibrations are also done by correcting for the differences between the crude correlator delay and recalculated precise delay including the troposphere and ionosphere. For maser sources, the Doppler velocity of the earth's orbital motion is also corrected for so that the radial velocities correspond to the LSR (Local Standard of Rest) velocity. After these calibrations, first we search for fringes of bright calibrator sources to find the clock offset and clock rate offset at each station. Then, the fringes are searched for the position reference source to obtain the fringe phases of the source. Usually the fringe phases are obtained at 1 min interval or less so that we can trace the short-term fluctuation of troposphere. After finding fringes of the position reference source, the source structure is imaged based on self-calibration process. Usually the self-calibrations are performed iteratively to solve the phases for the first run and to solve both phases and amplitudes for the later run. This is a typical analysis and mapping of normal VLBI observation (i.e., single-beam VLBI observation).

[1] http://hpiers.obspm.fr/eop-pc/

After the imaging of the position reference source is completed, the residual visibility phases (i.e., station-based solutions) are transferred to the paired target maser sources. When performing the phase corrections using the dual-beam data, the instrumental delay difference in the dual-beam system at each station is also corrected for. After these phase calibrations, phase-referenced visibilities of target maser sources are Fourier transformed to produce dirty images of each velocity channel. Finally, if a maser emission is detected in dirty images, the images are CLEANed and positions of maser spots are measured in the obtained images.

3. Examples of Phase-referencing Analyses

In the present section, in order to show how the phase referencing analyses have been conducted in VERA's astrometry, we present a typical example of VERA's phase referencing observation and its analyses. We take one of the multi-epoch observations of ON2N conducted from 2006 to 2008, for which astrometric results have been recently published by Ando et al. (2011). The reason for taking ON2N data here is that this maser is bright enough (~400 Jy), and the paired position reference J2015+3710 is bright as well (~0.8 Jy). Thus, thermal errors in visibility phases are small and hence one can clearly trace the phases in phase-referencing reductions.

3.1. Observation

Here we present the data obtained on the day of year 9 (January 9) in 2007. The observation was done using the full 4-station array of VERA. The target H_2O maser of ON2N at 22 GHz and the position reference source J2015+3710 were simultaneously observed using the dual-beam receiving system. The separation angle of the source pair is 1.27°. The duration of the observation was about 10 hours, and the on-source integration time for the target pair was 6 hours. The left-hand circular polarization was recorded onto the magnetic tape at the total recording rate of 1 Gbps, which provided a total bandwidth of 256 MHz. Using the VERA digital filter the received data are filtered into 16 sets of 16-MHz sub-bands. One 16-MHz sub-band is allocated for the target H_2O maser, and the remaining 15 of 16-MHz sub-bands are allocated for the continuum source (the position reference). Correlation processing was carried out with the Mitaka FX correlator, providing the spectral resolution of 15.625 kHz for the maser sub-band (corresponding to 0.21 km s^{-1} in the velocity resolution). We note that the setup of the observation is typical for the H_2O maser astrometry with VERA.

3.2. Reductions

Here we present the details of analyses of phase-referencing data obtained with VERA. We have developed a new software package called VEDA (VEra Data Analyzer), and the results presented here were produced with VEDA. However, the basic procedures of VEDA analyses are the same to those with other software, such as AIPS (Astronomical Image Processing System), basically consisting of calibrations, fringe searches, self-calibration imaging of the reference source, phase-transfer to the target, and phase-referenced mapping, as summarized in the previous section.

As a result of the single-beam mapping of the position reference source, through figures 1 to 4 we present the results of self-calibrations. Figure 1 shows the CLEAN map obtained with the self-calibration, and figure 2 shows the UV distance plot. We note that here the self-calibration solutions are obtained with an integration time of 32 sec. As seen in figure 1, the source J2015+3710 is nearly point-like, with a peak brightness of 0.83 Jy/beam. However, figure 2 also tells that there are weak structural effects in this source, which cause variations of visibility amplitudes between 0.7 and 1 .0 Jy depending on the baseline length. Figures 3 show the observed and model visibilities (amplitudes and phase) after subtracting the station-based phase solutions. We note that after the self-calibrations, the visibility phases are solved for the station-based ones and baseline-based ones. While the station-based phases consist of clock and clock rate offset as well as short-term phase-fluctuations caused by the troposphere, the baseline-based phases include the structure effect. Hence, by comparing the baseline-based visibilities with the model calculation based on the CLEAN components, one can test whether the self-calibration process worked properly or not. In the current case, after the self-calibration in figures 3 the visibilities are modeled well by the CLEAN components. Thus, figures 3 demonstrate that the self-calibration process worked well for this source. In fact the observed and modeled phases are consistent within a few degree levels, and the differences appear random without systematics. We note that this phase scatter is most-likely caused by the thermal noise. In fact, using the parameters in the present reduction such as the integration time of 32 sec, the bandwidth of 240 MHz, T_{sys} = 150 K and so on, the baseline-based noise level becomes σ_N = 24 mJy (1-σ), and hence the source with 0.8 Jy is detected at S/N of ~33, corresponding a phase noise of 57.3/33 = 1.7 deg. Therefore, the results

presented here confirm that the fringe search and self-calibration are conducted properly without systematic phase errors greater than the thermal noise level. Figure 4 shows the gain correction factor obtained in the self-calibration. As can be seen in figure 4, the gain correction factor is concentrated around unity within a scatter of 10-15%, indicating that the amplitude calibration with T^*_{sys} is done at this level.

After the self-calibration process, the station-based phase solutions are transferred to the target maser visibilities. When correcting for the phase of the target maser visibilities, the reference frequency difference between the position reference source and the target maser at each velocity channel is considered. Also, the dual-beam delay differences, which is monitored based on the horn-on-dish method at each station, were applied to the visibility phases. Once these key calibrations in VERA's phase-referencing are done, the visibilities of the target maser source are Fourier transformed to the dirty image and CLEANed. Figure 5 shows an example of CLEAN map of ON2N H_2O maser, detected at $V_{LSR} = -3.79$

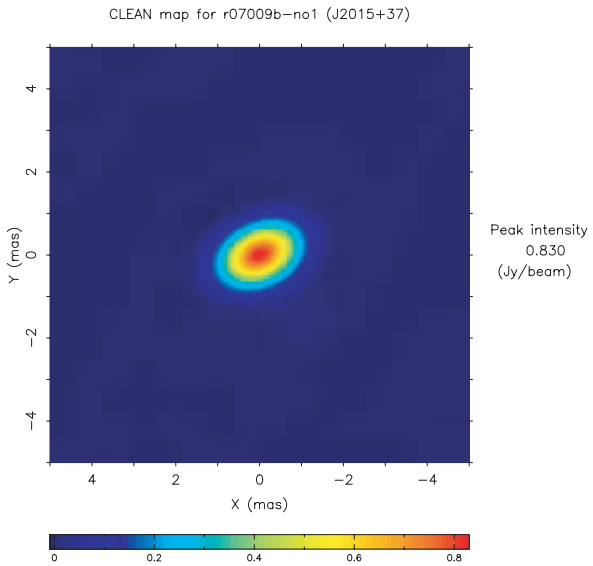

Fig. 1. Self-calibration map of the position reference source J2015+3710. In the self-calibration process, both the amplitude and phases are calibrated.

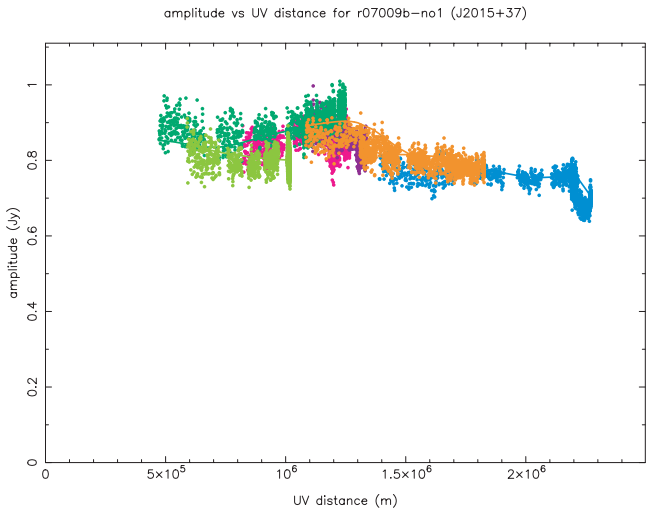

Fig. 2. UV distance plot for J2015+3710 after the self-calibration. Different color codes correspond to six baselines of VERA. Dots are the calibrated data and curves are the model calculated from the CLEAN components.

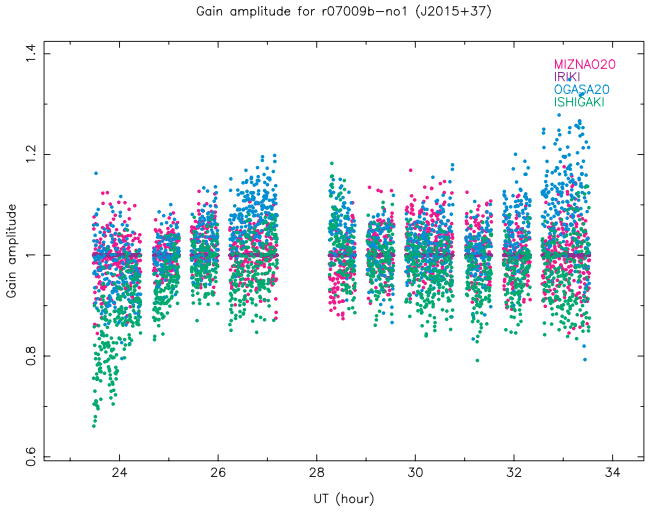

Fig. 4. Amplitude of the complex gain solved for each station based on the self-calibration of J2015+3715. The amplitudes are consistent with unity with a scatter of 10-15%. Note that Iriki station is the reference antenna and thus its gain is identical to unity at any time.

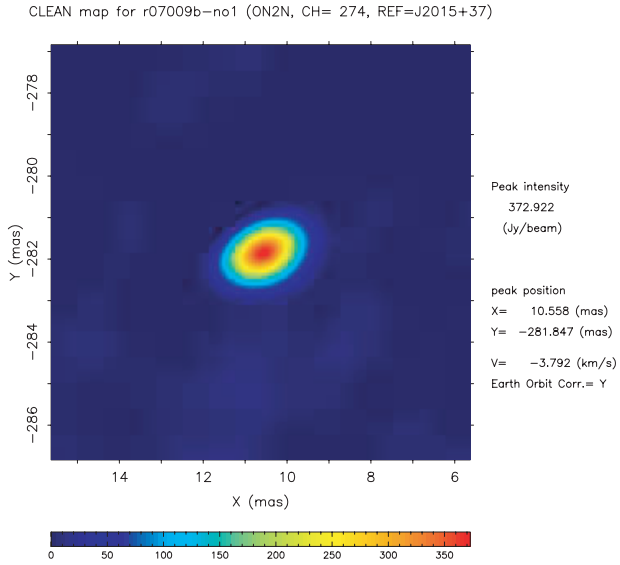

Fig. 5. Phase-referenced map of a spot of ON2N H_2O maser. The image is obtained by the Fourier transformation of phase-referenced visibilities and the CLEAN process.

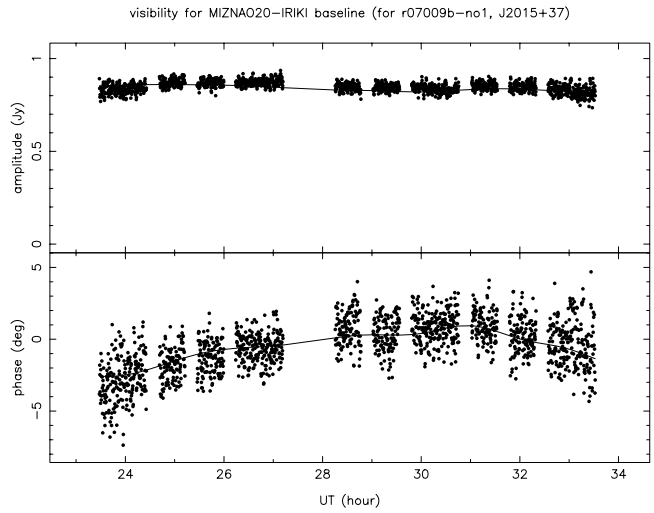

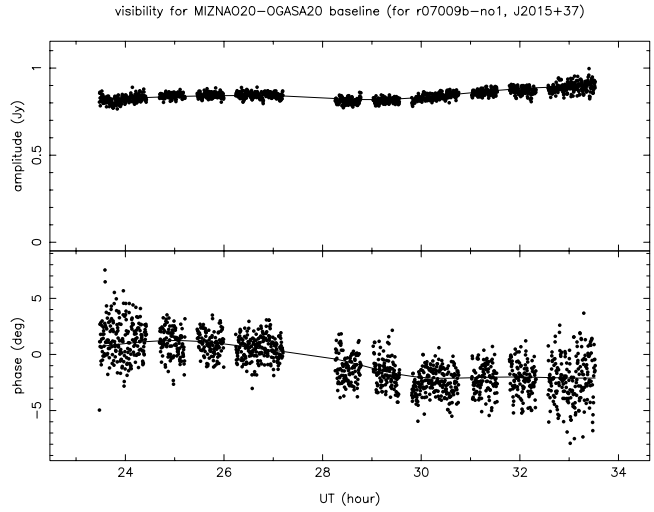

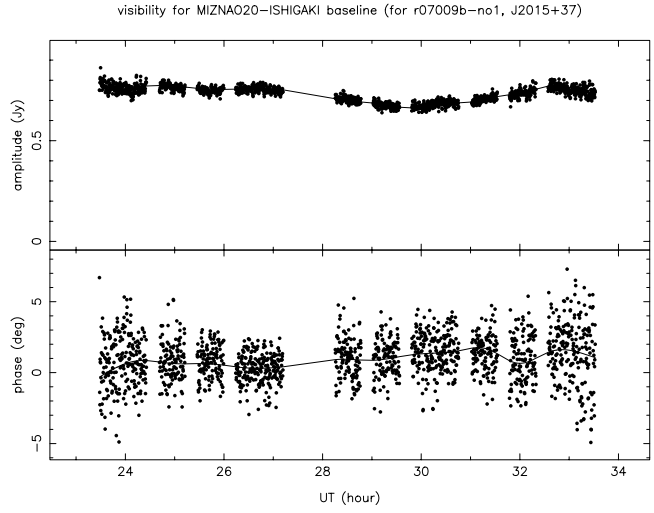

Fig. 3. (a: Top): The model (curve) and observed (dot) visibilities of J2015+3710 for the Mizusawa-Iriki baseline. The model visibilities are obtained from the CLEAN components of the self-calibration map. The observed visibilities are corrected for the station-based gain solutions obtained with the self-calibration. The upper panel shows the visibility amplitudes, and the lower panel shows the phases, respectively. (b: Middle): The same to figure 3a but for Mizusawa-Ogasawara baseline. (c: Bottom): The same to figure 3a but for Mizusawa-Ishigaki-jima baseline.

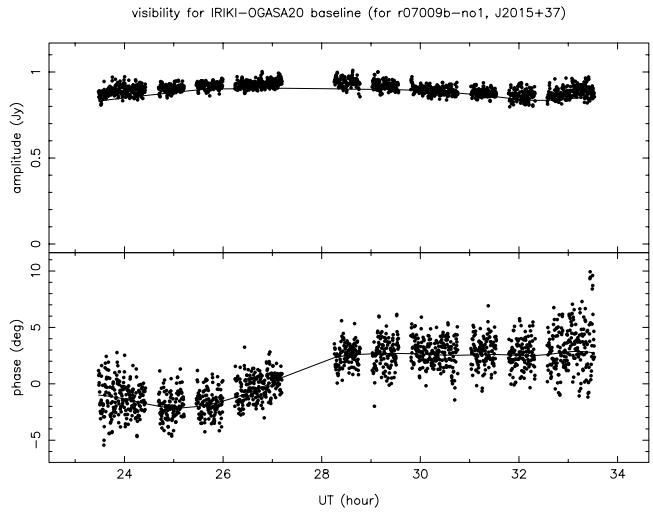

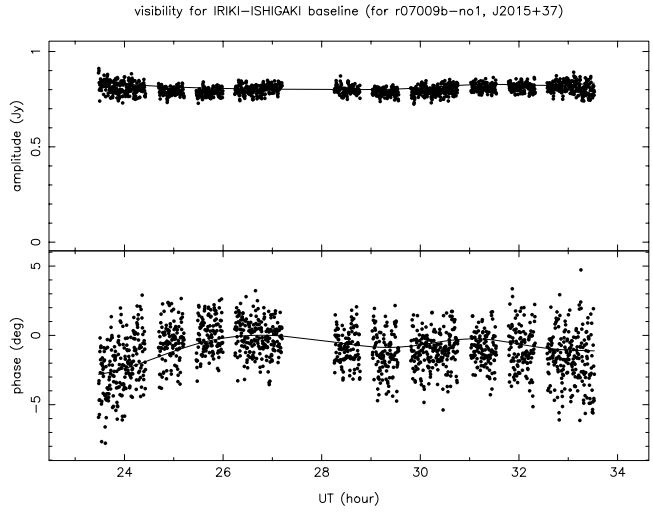

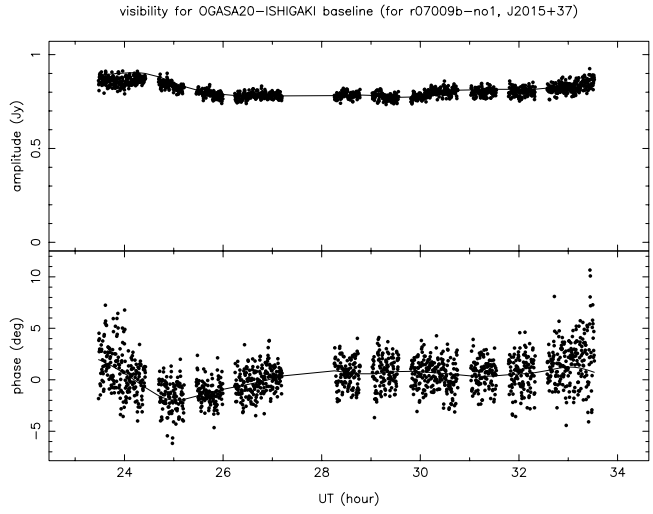

Fig. 3. *continued* (a: Top): The same to figure 3a but for Iriki-Ogasawara baseline. (b: Middle): The same to figure 3a but for Iriki-Ishigaki-jima baseline. (c: Bottom): The same to figure 3a but for Ogasawara-Ishigaki-jima baseline.

km s^{-1}. Here we take this spot as a sample for further analyses of phase residuals because this is one of the brightest spots in the map (peak intensity of 372 Jy/beam) and looks point-like, showing no distinct structure in the CLEAN map. In the usual phase-referencing astrometry with VERA, we create the CLEAN maps for all the velocity channels which contain the maser emissions, and the maser position are obtained from the CLEAN map (usually taking the intensity peak or fitting the intensity distribution). The final product of the data reduction for one epoch is the list of maser spots with positions, velocities, intensities etc. By combining the multi-epoch results of maser astrometry, one can perform astrometric analyses such as obtaining parallaxes and proper motions of maser sources.

3.3. *residual phase and Allan Standard Deviation*

In usual analyses, the data reduction ends with measuring the maser spot positions as described above. However, since the purpose of the present paper is to evaluate the performance of VERA in phase-referencing astrometry, here we further discuss the behavior of residual phases after the phase-referencing. Figure 6 shows the residual phases of ON2N H_2O maser at $V_{LSR} = -3.79$ km s^{-1}, after the correcting for the phase variation caused by the position offset of the spot, which is obtained to be $(X,Y) = (10.56, -281.85)$ mas (with respect to the tracking center position used in the correlation). These residual phases presented here should contain all kinds of phase errors which are not corrected for properly, and the structural effect of the maser spot as well (if there is any structure).

In figure 6, residual phases are basically concentrated around 0 with a scatter of ~20 deg, except the beginning and end of the observation. The large scatter and/or systematic phase drift at the beginning and end of the observation are due to the low elevation of the source: toward low elevations, the system noise temperature becomes high, and in addition the effect of tropospheric delay offset becomes significant, as seen from equation (1). These data may be flagged out by setting an elevation angle limit for valid visibilities.

To evaluate the performance of phase-referencing, here we calculate the Allan Standard Deviation (ASD) for the residual phases. The ASD can be calculated as

$$\sigma_y^2(\tau) = \frac{\langle [\phi(t+2\tau) - 2\phi(t+\tau) + \phi(t)]^2 \rangle}{8\pi^2 \nu_0^2 \tau^2}, \quad (2)$$

where ν_0 is the frequency, ϕ is the phase, τ is the time interval, and the bracket <> denotes the average over the whole samples. Figure 7 shows the ASD for the residual phases in figures 6. To eliminate the data at low elevations, here we used the data in figure 6 between UT 24.5 hour to 32.5 hour. In figure 7 the results from the six baselines of VERA are averaged, and the error bars are obtained as the scatter of the six data points at each time-interval τ. As seen in the figure, the ASD decreases with the time interval τ as $\sigma_y(\tau)$

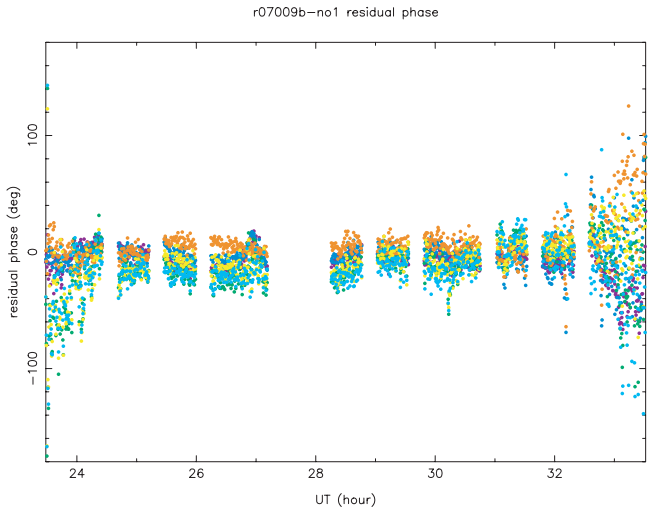

Fig. 6. Residual visibility phases of ON2N maser mapped in figure 5. Here the visibility phases are corrected for the position offset obtained by the phase-referencing map, and thus include the structural effect of the maser spots as well as the calibration residuals.

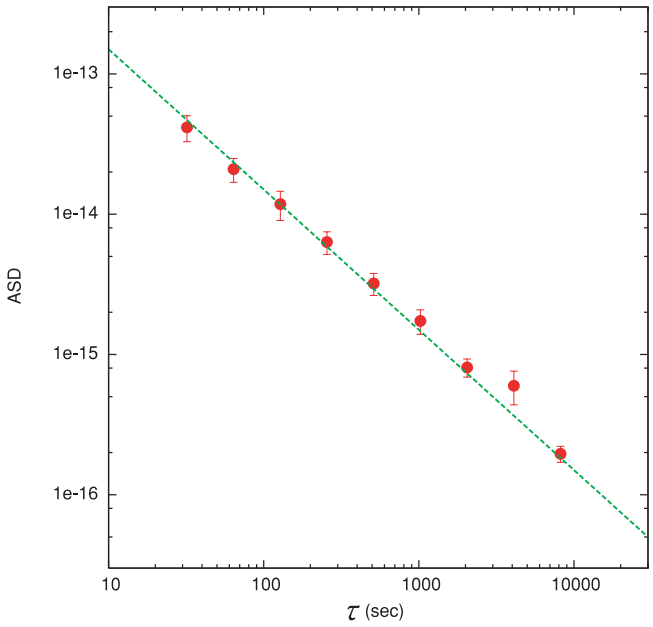

Fig. 7. Allan Standard Deviation (ASD) of the phase residuals obtained by using the data between UT 24.5 to 32.4 in figure 6. Here the ASD is obtained for each baseline and averaged over the six baselines. The error bars show the scatter of the ASD among the six baselines of VERA. The green line shows the behavior of the white-phase noise, characterized as $\sigma_y \propto \tau^{-1}$.

$\propto\tau^{-1}$, which is the behavior of the white phase noise. This is in contrast to the fact that the tropospheric phase fluctuation behaves as the flicker frequency noise, characterized as $\sigma_y \sim$ const. up to $\tau \sim 100$ sec (e.g., Thompson et al. 2001; Honma et al. 2003). In figure 7 there is no such constant "plateau" in σ_y caused by troposphere, and the white-phase noise behavior of the residual phase indicates that the tropospheric phase fluctuations were effectively cancelled out by the phase-referencing. This result is identical to what has been shown in Honma et al. (2003), confirming the results in the previous work. However, we note that here we used 8 hour data while the analyses of Honma et al. (2003) was limited up to 1 hour due to lacks of precise calibrations in that period. Therefore, the results presented here demonstrate the effectiveness of VERA's phase-referencing for a longer term, corresponding to a duration of a full-track observation. The ASD behavior of the white phase noise obtained in figure 7 is likely to be originated from the thermal noise of the pair sources and also the imperfections of the phase-referencing calibration. For the source pair of J2015+3710 (0.8 Jy) and ON2N maser (370 Jy for the maser spot considered here), the thermal noise of the continuum source J2015+3710 is dominating in the total thermal noise after the phase referencing. The expected ASD for the thermal noise of J2015+3710 is $\sim 1.4\times10^{-14}$ at $\tau=32$ sec. On the other hand, the measured ASD at $\tau=32$ sec in figure 7 is 4.2×10^{-14}, being three times larger than the thermal noise. This difference should be originated from other effects such as maser structures (note that in figure 6, the maser structure effect is not removed) and/or impefection of the phase calibration between the target and reference sources (i.e., difference of phase fluctuations toward the target maser and the position reference).

We note that by re-analyzing the data in Honma et al. (2003) Miyoshi (2009) claimed that the VERA's phase-referencing did not work effectively beyond 1 hour. However, in Miyoshi (2009) the proper calibration processes, which are conducted in this paper, were not fully performed: for instance, the observations in Honma et al. (2003) were test observations with only one baselines, and thus the structure effect of the reference source cannot be removed by the self-calibration. Also, in these data, the dual-beam instrumental delay differences as well as recalculation of precise delay were not implemented, and the calibrations of such delays were not taken into account in Miyoshi (2009). Therefore, it is rather natural that the phase-residual beyond 1 hour would have some systematic trend different from the 24-hour sinusoidal variation (which is caused by the position offset and provides astrometric information of the source), and hence we point out that the treatment of data as well as the conclusions in Miyoshi (2009) were irrelevant. As shown in the present paper, only proper calibrations can lead to the residual phases that are nearly white-phase noises, being in agreement with the result presented in Honma et al. (2003).

4. Error in Calibration and Astrometry

In this section, we evaluate calibration errors and their effect on astrometry. Basically astrometric accuracy of phase-referencing VLBI is related to the calibration error (i.e. phase residual) and the baseline length as

$$\Delta\theta=\frac{c\Delta\tau}{B}. \tag{3}$$

Here $\Delta\theta$ is the position error in astrometric measurement, $c\Delta\tau$ is the calibration error described in the path length, and B is the maximum baseline of the array, for which we adopt 2300 km for the VERA array in the present paper. The calibration error $c\Delta\tau$ consists of different types of error sources, and here we discuss the details below.

4.1. Short-term phase residuals

As presented in the previous section, the short-term phase fluctuations are cancelled out effectively by utilizing the dual-beam observations, and remaining phase residuals after the phase referencing can be reduced down to a few times of the thermal noise level. The case shown in the previous section is for a bright source pair, and in other cases the thermal noise could be worse than that in the case shown in the previous section. Assuming typical source fluxes for VERA observations (100 mJy for continuum and 15 Jy for masers, in which the continuum source is limiting the signal-to-noise ratio) and assuming typical parameter of VERA's observations at 22 GHz ($T_{\rm sys}=150$ K), the baseline-based fringe detection limit is 85 mJy for S/N=5 (assuming 60 sec integration time and 240 MHz bandwidth). Since the fringe phase uncertainty is provided by the inverse of the signal-to-noise ratio (i.e., $\sigma_\phi=1/{\rm SNR}$), such a source has an phase error of $\sim 1/5$ rad., or 11 deg. Thus, after combining the whole observations (typical on-source integration period of 4 hours), the mean of fringe phase for each baseline can be obtained with an accuracy of 11 deg/$\sqrt{4\times3600/60}=0.7$ deg. This corresponds to the path length residual of 0.03 mm. Assuming that the residual after phase-referencing is three times larger than the thermal noise level as shown in the previous section, the path length residual should be $c\Delta\tau_{\rm thermal}$

~0.09 mm. We note that in some extreme cases, the masers are so faint that they can only be detected in the phase-referenced map after the integration of hours. In such cases, the astrometric accuracy will be basically determined by the map dynamic range $R_{\rm dyn}$ and may be written as $\Delta\theta \approx (\theta_{\rm beam}/2/R_{\rm dyn})$, which might give a worse error than the above estimates.

4.2. Zenith delay offset

The zenith delay offset is long-term variable and this term causes a position offset in astrometry through the air mass difference between the target maser and position reference. For instance, Honma et al. (2008b) presented the calibration of the zenith delay offset using GPS and revealed that the zenith delay can be measured at 2-cm level. For source separation of 1 deg, a rough estimate of a path length error is given by 20 mm × 1/57.3 = 0.35 mm. Of course this is a crude order-estimate and the exact value depends of the elevation angle (EL) difference of the sources and the mapping function of the troposphere (which basically depends only on EL and is independent of the azimuthal angle AZ). However, according to the detailed studies of the astrometric effect of the zenith delay offset by Honma et al. (2008b), for relatively high elevation sources (such as $\delta \geq 15^\circ$), the order-estimation obtained above provides a reasonable measure for the position uncertainty due to the zenith delay offset. Also, it is shown that the effect of the zenith delay offset is proportional to the separation angle of the source pair $\theta_{\rm SA}$, so one can scale the path length error caused by the zenith delay as

$$c\Delta\tau_{\rm tropo} = 0.35 \times \left(\frac{\theta_{\rm SA}}{1\ {\rm deg}}\right) {\rm mm}. \quad (4)$$

4.3. Ionosphere

Ionospheric effect is dispersive (scales with ν^{-2}) and thus more prominent in lower frequency. Its phase delay is calculated as

$$\Delta\tau_{\rm iono} = -\frac{cr_0}{2\pi\nu^2} I_{\rm e}, \quad (5)$$

where r_0 is the classical electron radius, and $I_{\rm e} = \int n_e dl$ is the total electron content (TEC). In case of astrometry with VERA, the ionospheric effect is more significant in 22 GHz than in 43 GHz. In VERA analyses we use the Global Ionosphere Map produced every 2 hour based on the international GPS network. Assuming a typical ionospheric condition over the VERA sites with a TEC value of 50 TECU (though TEC is variable depending on the Solar activity etc., note 1 TECU = 10^{16} electrons m^{-2}), the phase delay for 22 GHz becomes ~4.2 cm. Usually, the TEC (Total Electron Content) measurements are thought to be accurate at 15% level. In that case, the TEC error causes ionospheric path uncertainty of 0.62 cm, and thus for a source pair with the separation angle of $\theta_{\rm SA} = 1$ deg, the delay residual can be written as

$$c\Delta\tau_{\rm iono} = 0.11 \times \left(\frac{\theta_{\rm SA}}{1\ {\rm deg}}\right) {\rm mm}. \quad (6)$$

4.4. Station position error

In the correlation process of VLBI data, delay and its variation are predicted based on the precise geodetic model and station positions. The visibility phases, which are the correlator output for the astrometric analyses, are corrected for the predicted delays. Since the baseline measured by the geodetic observations could include some errors, it propagates to the visibility phase errors through the model delay calculations. In VERA, geodetic VLBI observations have been regularly conducted nearly twice a month and station positions are measured at 3mm level (Jike et al. 2009). If we assume the separation of one degree for the maser-QSO target pair of VERA, the station position error causes delay error as $c\Delta\tau_{\rm geo} = 3/57.3 = 0.05$ mm, and this linearly scales with the separation angle of the maser-QSO pair. Therefore, the calibration error due to the station position error is written as

$$c\Delta\tau_{\rm geo} = 0.05 \times \left(\frac{\theta_{\rm SA}}{1\ {\rm deg}}\right) {\rm mm} \quad (7)$$

We also note that there could exist some errors in the geodetic model itself (such as the models in the earth tides and/or earth rotation measurements etc) rather than the measured station positions. However, according the most modern geodynamical model (e.g., IERS 1996, 2000 etc), the model uncertainty is expected to be less than 3 mm, and hence here we only consider the station position errors.

4.5. dual-beam instrumental delay

Since VERA telescopes utilize the dual-beam receiving system to observe a source pair, the paths in the instrument (in antenna, receivers, cables, digital backends etc.) are totally different for the two objects. Therefore, one has to calibrate the path length difference between the dual-beam receiving

system. This calibration is done on real time during the observations by monitoring the common noise injected into to the dual-beam receivers. Details of this calibration technique is summarized in Honma et al. (2008a), and the main conclusion there is that the path length difference can be calibrated at an accuracy of $c\Delta\tau_{ins} = 0.12$ mm. This evaluation was done at the separation of 2 degree, and hence this provides nearly worst case. It is likely that this calibration error also linearly scales with the separation angle of the dual-beam, but in the present paper we conservatively assume that the calibration error in the dual-beam path length difference is independent of the separation angle, being constant of 0.12 mm. Hence we can write the instrumental delay residual as

$$c\Delta\tau_{2B} = 0.12\text{mm} \quad (8)$$

4.6. *Source structure*

The source structure and its variation can also affect the astrometric results. Here the term "source structure" include the structure and variation of the position reference and target maser sources. However, since the source structure effect does not exist in the observing system such as instruments and propagation but exists in the sources themselves, here we treat their effects separately from the calibration errors, and we will discuss their effects in the next section in details. Thus, in this section, the astrometric error considered here can be regarded as that for point sources.

4.7. *Total error*

By combining the errors presented above, here we consider the total error in calibration as well as astrometry with VERA. Table 1 summarizes the calibration error and their dependences on θ_{SA}. As seen in table 1, the dominant factor is the tropospheric zenith delay offsets. In case of the separation angle of 1 deg, the RSS (root-sum-square) of the calibration error becomes 0.40 mm, most of which comes from the zenith delay offset. Using the maximum baseline length of 2300 km for VERA, this provides an astrometric uncertainty of $0.40/2.3\times10^9 = 34$ μas. Or, for 2-degree separation case, the path error becomes 0.79 mm, corresponding to an astrometric uncertainty of 69 μas. Note that this astrometric error corresponds to that of the measurement with one epoch. In measuring the parallax and proper motions, data of multiple epochs are combined. For instance, in VERA observations sources are regularly monitored every one or two months. Since the dominant calibration error, the zenith delay offset, is expected to be random between epochs, the use of multiple epochs reduces the error of the parallax statistically with $\sigma \propto 1/\sqrt{N}$, where N is the number of epochs. Thus using $\sim$10 observations, one can reduce the parallax error by a factor of 3 compared to the astrometric error in each epoch. Therefore, under relatively good conditions such as high elevation and small separation angle (e.g., less than $\sim$ 1 deg), one can expect a parallax accuracy of 10 μas. On the other hand, for sources with worse conditions, the parallax error should exceed 10 μas, but astrometry at 20 μas-level is still feasible for sources with 2-deg separation if the source elevations are high. This is the current best estimate of VERA's astrometric performance. The results presented here are consistent with the observational results of VERA, in which parallax measurements were done at 10 μas level for some sources under relatively good conditions (e.g., S269 by Honma et al. 2007, ON1 by Nagayama et al. 2011a, ON2N by Ando et al. 2011).

5. Source Structure Effect

In the previous section, we focused on the effect of calibration errors on the astrometric results assuming that sources are point-like. However, in practice, any astronomical object could have source structures, and in many cases for VERA, the structures vary with time. In fact, the target sources of VERA are maser sources and AGN cores, both of which are known to have structures and their variations with a time scale of months to years. Therefore, in addition to the calibration errors (which are mainly originated from the

Table 1. Summary for sources of errors in calibration normalized at a separation of 1 deg.

error source	$c\Delta\tau$	θ_{SA} dependence	note
short-term phase error	0.09 mm	—	estimated as three times the thermal noise
tropospheric zenith delay	0.35 mm	$\propto\theta_{SA}$	for relatively high Dec. source
ionosphere	0.11 mm	$\propto\theta_{SA}$	
station position	0.05 mm	$\propto\theta_{SA}$	
dual-beam instrumental delay	0.12 mm	—	
RSS (for $\theta_{SA} = 1$ deg)	0.40 mm	$\sim\propto\theta_{SA}$	corresponding to position error of 34 μas

instruments and propagation of electromagnetic wave), the source structure effects should be also considered when discussing the total astrometric accuracy. Hence here we consider the structures of both position references and target masers and discuss their effects on the astrometry.

5.1. *Position reference structure*

In typical analyses of VERA, the fringes are first searched for the position reference sources and its image is obtained based on the self-calibration. Therefore, the structure effect of the position reference can be solved and removed. For instance, the observed and the modeled phases are shown in figures 3 for the case of J2015+3710. Figures 3 clearly demonstrated that the phases from the structure are well-modeled and thus effectively separated from the other phase errors such as due to tropospheric delays and instrumental delays. This indicates that as a first order approximation, the structure effects of the position reference are removed out when the station-based phase solutions are transferred to the visibilities of the target maser source in the phase-referencing analyses.

On the other hand, AGN cores often show so-called core-jet structure in which the jet component moves away from the radio core. This kind of structure variation caused by the jet motion could introduce uncertainty in astrometry. If the core and jet are clearly separated in the image, then the structural effects should be mostly removed by conducting the self-calibrations, as argued above. However, if the core and jet components are so close that the two components cannot be distinguished in the image, then the jet motion causes the variation of intensity peak position in the AGN map, and thus could affect the results of the phase-referencing astrometry. Assuming that the jet-core structure is not separated within a monitoring period of VERA (which is typically a year), the jet-core separation that should be considered here is an order of ~0.1 mas, which corresponds to 1/10 of the VERA's beam at 22GHz and thus indistinguishable in the map. In many cases of AGN jet, their motions can be approximated as ballistic, and the centroid shift is expected to be roughly linear with time. Therefore, in case that the position reference possesses the unresolved core-jet structure with ballistic jet motion, this causes a linear centroid shift with time, and thus causes systematic error in the proper motion rather than error in parallax. A rough estimate of the proper motion error introduced by an unresolved core-jet motions is an order of ~0.1 mas/yr. For a source at the distance of 8 kpc, this corresponds to a velocity of 4 km s^{-1}, being significantly smaller than the Galactic rotation velocity of ~220 km s^{-1}.

5.2. *Maser Structure*

In usual analyses of VERA, first fringe searches are done for the position reference sources, and the maser spot images are obtained in the phase-referenced map. Thus, the self-calibration procedure is not applied to the maser spot maps. Therefore, the phase-referenced visibilities of maser sources include both the phase offsets caused by the position and those caused by the structure of maser spot itself. Hence the structure of the maser spot could also cause systematic error in astrometry. If the structure is invariant with time, the position offset should be constant and thus the structure effect does not cause any error in astrometry. However, maser sources are also known to be time-variable, with flux and structure variations with a time-scale of a few months to years. Therefore, such maser structure variation could introduce additional errors in astrometric measurements.

Here we evaluate the effect of maser structure variation assuming that the position of the maser intensity peak varies due to the turbulent motion in the maser-emitting gas clouds. Usually maser lines have a velocity width less that 1 km^{-1}, and hence the amplitude of the turbulent motions in the gas clouds are likely to be this order or less. Assuming a systematic motion of maser intensity peak at 0.5 km s^{-1} for a year, the maser peak position can varies by 0.5 km $s^{-1} \times 1$ yr = 0.1 AU. On the other hand, the parallax corresponds to an angular size of 1 AU at the source distance, and hence a very rough estimate here suggests that the maser turbulent motion could causes a parallax error of ~10%. However, of course the maser turbulent motion should not necessarily cause sinusoidal motion like a parallax, but is expected to be more or less random. Hence, the parallax error is expected to be better by a factor of a few than the above estimate, and thus it is expected that the maser structure variation causes parallax error of 3-10% level. We note that this structure effect is independent of the maser distance, and hence under the existence of such a turbulent motion of the maser intensity peak, the parallax accuracy should be always 3-10% for any sources. Therefore, the effect of the maser structure on astrometry is quite different from those caused by the calibration errors, and it can be another source of errors in addition to those discussed in the previous section.

5.3. *Testing the structure effects in VERA's results*

In order to evaluate if the maser structure effects can

be seen in the astrometric results of VERA, here we discuss the accuracies of parallaxes obtained with VERA. We compiled data of parallax measurements obtained for the following sources: G14.33-0.64 (Sato et al. 2010), G34.3 + 0.1 (Kurayama et al. 2011), SY Scl (Nyu et al. 2011), G48.61 + 0.02 (Nagayama et al. 2011b), IRAS 19213 + 1723 (Oh et al. 2010), K3-35 (Tafoya et al. 2011), ON1 (Nagayama et al. 2011a), ON2N (Ando et al. 2011), AFGL 2789 (Oh et al. 2010), IRAS 22198 + 6336 (Hirota et al. 2008b), NGC 281 (Sato et al. 2008), L1448C (Hirota et al. 2011), NGC 1333 (Hirota et al. 2008a), IRAS 05137 + 3919 (Honma et al. 2011), IRAS 06061 + 2151 (Niinuma et al. 2011), S269 (Honma et al. 2007), Orion KL (Hirota et al. 2007), VY CMa (Choi et al. 2008), S Crt (Nakagawa et al. 2008), IRAS 16293-2422 (Imai et al. 2007). In figure 8 we show the plot of the parallax versus the parallax error for the maser sources listed above. The red spots in figure 8 correspond to the parallaxes obtained with a single spot, and the green spots correspond to the parallaxes obtained with a combined fit to multiple maser spots (in which a common parallax is obtained from the whole maser spots). As shown in figure 8, there is a strong correlation between the parallax amplitude and the parallax error, showing a linear relation (i.e., $\sigma_\pi \propto \pi$). In other words, the parallax error are mostly around 5-15%, being independent of the amplitudes of the parallaxes. The calibration errors in observing system can never produce this dependence of σ_π on π. On the other hand, this strong correlation can be interpreted in terms of the maser structure effect: as discussed in the previous subsection, the motion of maser peak intensity at 0.5 km s^{-1} for a year can cause an positional error corresponding to 0.1 AU scale, corresponding to a parallax error of ~10%. Therefore, the strong linear correlation between σ_π and π clearly show that the maser structure effects are significant in VERA's astrometry.

On the other hand, as discussed in the previous section, the calibration error is likely to be dominated by the tropospheric zenith delay. If this is the dominant error source in astrometry, we should see a correlation between the parallax error σ_π and the separation angle of the target and reference source θ_{SA}. This expectation was confirmed by the simulation done in Honma et al (2008b), demonstrating that the astrometric error σ_π should scale linearly with the separation angle θ_{SA} (in the absence of structure effects). To test this correlation in the real data, in figure 9 we show the plot of σ_π against θ_{SA} for the same data with those in figure 8. In figure 9, the correlation between σ_π and θ_{SA} is not prominent. For references, we also show in figure 9 the two regression lines with $\sigma_\pi = const.$ and $\sigma_\pi \propto \theta_{SA}$, but the lines do not provide significant difference in the fitting residuals, indicating that there is only week correlations between σ_π and θ_{SA}. This is in contrast to what we have found in figure 8 (i.e., strong correlation between σ_π and π).

The results present in figures 8 and 9 can be interpreted as follows. In VERA data, the structure (and its variation) of

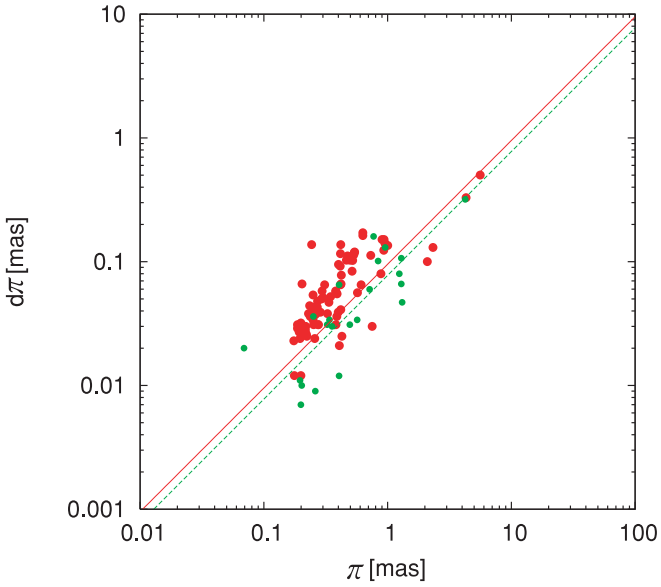

Fig. 8. Parallax amplitudes π versus parallax errors σ_π in VERA's results. Red spots are the results obtained by using one spot data, and greens spots are those by combined fit to multiple maser spots. Regression lines (in the form of $\sigma_\pi = a\pi$) for red and green spots are also shown.

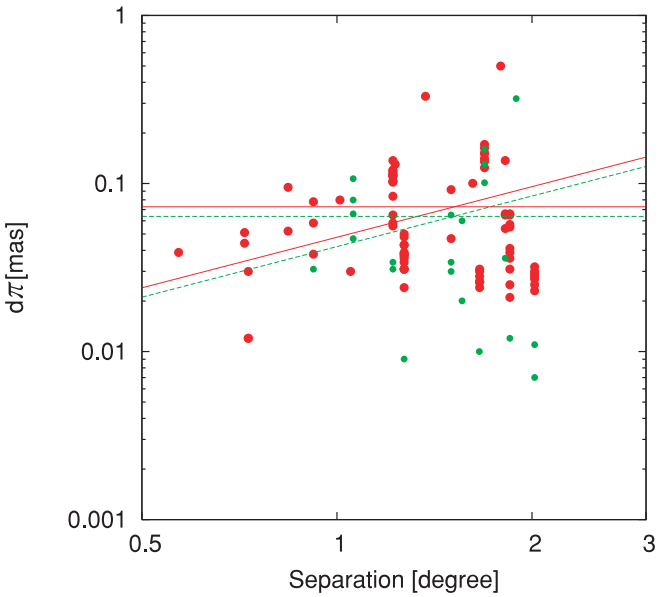

Fig. 9. Pair separation angle θ_{SA} versus parallax errors σ_π in VERA's results Spot color is the same to those in figure 8. Two regression lines (in the form of $\sigma_\pi = a\theta_{SA}$ and $\sigma_\pi = const.$) are shown, but these two lines do not provide significant difference in the fit.

the maser is a significant source of the astrometric error, and this limits the parallax accuracy at 5-15% level. This is understandable when one considers that most of sources for which parallaxes have been detected are not so distant, mostly within a few kpc from the Sun. For instance, for a source at D = 2 kpc, 10% of the parallax amplitude becomes 50 μas, which is larger than the expected astrometric error from the calibration errors in the observing system (i.e., $30\mu as/\sqrt{N}$ for $\theta_{SA} = 1$ deg, where N is the number of epochs). Therefore, for such sources, the calibration errors are less significant than the contributions of maser structure, and thus one can explain the trends found in figures 8 and 9. On the other hand, for more distance sources (i.e., D≥3kpc) the maser structure effect and the calibration errors in the system become comparable. The fact that the declination errors in astrometry tend to be larger than the right ascension errors (e.g., Honma et al. 2007) support the idea that the calibration error is also contributing to the astrometric error: as seen in the previous section, the calibration error is dominated by the tropospheric zenith delay, which mainly causes the position offset in the declination (e.g., Honma et al. 2008b). For most distant sources (D～10 kpc), it is expected that the dominant sources of astrometric error would be the calibration errors, and only for these sources there would be a correlation between σ_π and θ_{SA}. At present, the number of distant sources for which parallaxes have been measured is not enough for testing correlations shown in figure 9 for such sources, but we have to increase more samples to reach at better conclusions.

The important conclusion from the discussion presented here is that the astrometric analyses using multiple maser spots are valid and a proper way to improve the parallax. While the calibration errors must be common to the multiple maser spots and thus cannot be cancelled out by averaging the results of multiple spots, the maser structure can be different between the maser spots (or perhaps at least different between maser features), and thus doing a combined fit for multiple spots with a common parallax is valid to obtain better parallaxes by reducing the structure effects of individual maser spots.

6. Conclusions and Future prospects

We have shown that the phase-referencing with the dual-beam system of VERA works effectively to cancel out the short-term tropospheric fluctuation. As shown in section 3, once proper calibrations are carried out, the phase-residual after the phase-referencing nearly becomes white-phase noise for a long term (i.e., nearly full track of ～8 hour), confirming and extending the previous finding by Honma et al. (2003) for rather short-term of ～1 hour. We have also discussed the sources of astrometric errors due to calibration errors, and found that in the absence of source structure, the tropospheric zenith delay is the dominant source of astrometric error. In such a case, VERA can achieve 10 μ-as level astrometry for sources with relatively good conditions by reducing the random error of troposphere based on multi-epoch astrometry for ～10 epochs. On the other, we have also discussed the effect of source structures, and found that the maser structure variation is another significant source of error in astrometry. Based on the real data of VERA, we have found that there is strong correlation between the parallax amplitude π and parallax error σ_π, indicating that in most cases of VERA's observations the parallax measurements are limited by the variation of maser structure (especially the position wander of the intensity peak), providing the parallax error of 5-15% independent of the source distances.

Based on the results obtained here, here we briefly describe the future prospect, in particular a possible way to improve the astrometric accuracy in the near future. As shown in equation (3), in the absence of structure effect, the astrometric error is obtained as the ratio of the calibration error over the baseline length. If there is no structure effect, then both reducing the calibration error (smaller $\Delta\tau$) and expanding the baseline length (larger B) can work to improve the accuracy. However, since in many cases the astrometric error is dominated by the structure effect, reducing the calibration error $\Delta\tau$ would not improve the astrometric results significantly. In contrast, extending the baseline will provide higher angular resolution, and thus it is also helpful to reduce the structure effects. Therefore, the better way to improve the astrometric accuracy is most-likely to extend the baseline rather than to reduce the calibration error (or both is better if possible). Since the short-term tropospheric fluctuation is not a dominant source of astrometric error, a baseline expansion even with a single-beam VLBI station (rather than dual-beam station like VERA) would be able to improve the astrometric performance by conducting fast-switching. To realize this, the array expansion by including stations in East Asia (such as Korean VLBI Network and Chinese VLBI Network) will be most effective, and the forthcoming East Asian VLBI Network (EAVN, including China, Korea and Japan) is promising for conducting better astrometry.

References

Ando. K., et al. 2011, submitted to *PASJ*

Choi. Y.K., et al. 2008, *PASJ*, **60**, 1007

Hirota. T., et al. 2007, *PASJ*, **59**, 87

Hirota. T., et al. 2008, *PASJ*, **60**, 37

Hirota. T., et al. 2008, *PASJ*, **60**, 61

Hirota. T., Honma. M., Imai. H., Sunada. K., Ueno. Y., Kobayashi. H., & Kawaguchi. N., 2011, *PASJ*, in press

Honma. M., Kawaguchi. N., Sasao. T., 2000, in Proc. SPIE Vol.4015 Radio Telescope, ed H. R. Buthcer, p624-p631

Honma. M., et al. 2003, *PASJ*, **55**, 57

Honma. M., et al. 2007, *PASJ*, **59**, 88

Honma. M., et al. 2008a, *PASJ*, **60**, 35

Honma. M., Tamura. Y., & Reid, M. J. 2008b, *PASJ*, **60**, 51

Honma. M., et al. 2011, *PASJ*, in press

Imai. H., et al. 2007, *PASJ*, **59**, 1107

Jike. T., Manabe. S., Tamura. Y., 2009, *Journal of Geodetic Society of Japan*, **55**, 369

Kawaguchi. N., Sasao. T., Manabe. S., 2000, in Proc. SPIE Vol.4015 Radio Telescope, ed H. R. Buthcer, p544-p551

Kurayama. T., et al. 2011, submitted to *PASJ*

McCarthy. D.D., 1996, IERS Tech. Note, No.21, p.1-95, 21, 1

Miyoshi. M., 2009, *PNAOJ*, **12**, 1

Nagayama. T., et al. 2011, submitted to *PASJ*

Nagayama. T., et al. 2011, submitted to *PASJ*

Nakagawa. A., et al. 2008, *PASJ*, **60**, 1013

Niinuma. K., et al. 2011, *PASJ*, in press

Nyu. D., et al. 2011, *PASJ*, in press

Oh. C.S., Kobayashi. H., Honma. M., Hirota. T., Sato. K., & Ueno. Y, 2010, *PASJ*, **62**, 101

Sasao T, 1996, in proceedings of 4th APT Workshop, ed. E. A. King, p94-p104

Sato. M., et al. 2008, *PASJ*, **60**, 975

Sato. M., Hirota. T., Reid. M.J., Honma. M., Kobayashi. H., Iwadate. K., Miyaji. T., & Shibata. K.M, 2010, *PASJ*, **62**, 287

Tafoya. D., et al. 2011, submitted to *PASJ*

Thompson A. R., Moran J. M., Swenson G.W.Jr. 2001, Interferometry and Synthesis in Radio Astronomy 2nd edition (Wiley-Interscience, New York)